

A multi-scale, mechanistic model of a wet granulation process using a novel bi-directional PBM–DEM coupling algorithm



Dana Barrasso ^a, Thomas Eppinger ^b, Frances E. Pereira ^c, Ravindra Aglave ^d, Kristian Debus ^e, Sean K. Bermingham ^c, Rohit Ramachandran ^{a,*}

^a Department of Chemical and Biochemical Engineering, Rutgers, The State University of New Jersey, Piscataway, NJ 08854, USA

^b CD-adapco, Nordostpark 3-5, Nuremberg 90411, Germany

^c Process Systems Enterprise Ltd., 26–28 Hammersmith Grove, London W6 7HA, UK

^d CD-adapco, 11000 Richmond Ave, Houston, TX 77042, USA

^e CD-adapco, California Office, CA, USA

HIGHLIGHTS

- A multi-scale, mechanistic model of a wet granulation process is developed.
- An efficient bi-directional coupling algorithm is implemented to exchange data between models.
- Particle-scale information from DEM simulations is used to evaluate rate expressions in the PBM.
- Sensitivities to process parameters, material properties, and equipment geometry are demonstrated.

ARTICLE INFO

Article history:

Received 19 August 2014

Received in revised form

21 October 2014

Accepted 3 November 2014

Available online 11 November 2014

Keywords:

Wet granulation

Population balance modeling

Discrete element methods

Multi-scale modeling

Quality-by-Design

ABSTRACT

In this study, a novel mechanistic model for a wet granulation process is presented, combining the techniques of population balance modeling and discrete element methods to predict critical quality attributes of the granule product, such as porosity and size distribution. When applied to a twin screw granulation process, the model shows sensitivities to the screw element type and geometry, as well as material properties (binder viscosity, pore saturation) and process parameters (screw speed, liquid-to-solid ratio). Predicted trends are consistent with experimental observations in the literature. Using this modeling framework, a model-based approach can be used to implement Quality by Design, establishing a design space to transition towards a quantitative mechanistic understanding of wet granulation processes.

© 2014 Elsevier Ltd. All rights reserved.

1. Introduction

Over the past decade, Quality by Design (QbD) has gained importance in the pharmaceutical industry to manage risk, reduce costs, and satisfy regulatory requirements. In 2006, QbD was introduced in the ICH Q8 guidance document and later was defined as “a systematic evaluation, understanding and refining of the formulation and manufacturing process” ([U.S. Food and Drug Administration, 2006, 2009](#)). In contrast, the traditional approach of Quality by Testing (QbT) involves empirical design and operation of manufacturing processes and relies on testing and rejection of failed batches to assure quality, which can lead to sub-optimal product quality.

To implement QbD, predictive process understanding must be established to quantify the effects of process parameters and material properties on the critical quality attributes (CQAs) of the product. From this knowledge base, a design space can be identified, defining the multi-variate combination of process parameters and material properties that result in a product of acceptable quality. Experimental approaches to QbD often rely on large sets of experimental data and statistical models, but provide little insight beyond the experimental design space.

Alternatively, a model-based approach can be taken to describe the behavior of the process from a more scientific perspective. The underlying mechanisms driving the process are described mathematically, and a limited number of experiments are required to calibrate and validate the model ([Kayrak-Talay et al., 2013](#)). The development of truly predictive pharmaceutical process models is challenging because many of these processes involve powders. Powder processes are often operated empirically and inefficiently

* Corresponding author. Tel.: +1 848 445 6278; fax: +1 732 445 2581.

E-mail address: rohit.r@rutgers.edu (R. Ramachandran).

due to a poorer understanding of their behavior compared to that of liquid and gas processes. This paper focuses on the development of a more predictive model for a wet granulation process.

Wet granulation is a key unit operation in tablet manufacturing in which a liquid binder is added to fine powder particles to form larger granules, improving flowability and compactibility, while preventing segregation of the solid components. This complex process is driven by several interrelated subprocesses: wetting and nucleation, aggregation and consolidation, breakage and attrition, and layering (Iveson et al., 2001). As liquid is added, fine powders form porous nuclei that can coalesce, deform, and break. These particles can also take up additional liquid or fine powder particles, altering their behavior.

Various types of equipment can be used for wet granulation, including high shear mixers, fluidized beds, and twin screw extruders. This study focuses on twin-screw granulation (TSG), which has potential advantages in continuous pharmaceutical manufacturing because of its low throughput, flexible design, and short residence time (El Hagrasly et al., 2013). However, the multi-scale modeling approach presented in this study can be applied to the general class of wet granulation systems.

1.1. Powder process modeling

Traditionally, models of wet granulation processes fall into one of two categories: process models or particle-scale models. Population balance modeling (PBM) is a process modeling framework that groups particles into classes based on their sizes and other properties, tracking changes in the number of particles in each class as they undergo rate processes, such as aggregation and breakage. PBMs have been used extensively to simulate wet granulation processes (Cameron et al., 2005; Verkoeijen et al., 2002). Multi-dimensional PBMs are particularly useful in tracking distributions of multiple particle properties, such as size, liquid content, and porosity, which can affect the aggregation and breakage rates in the system (Immanuel and Doyle, 2005; Poon et al., 2008).

The development of accurate descriptions of aggregation and breakage rate expressions is an area of significant research. Many rate kernels are empirical and require estimation of unknown parameters from experimental data. Parameter estimation and validation have been performed for wet granulation processes, but these calibrated models have limited predictive capabilities outside of their experimental design spaces (Braumann et al., 2010; Ramachandran and Barton, 2010; Man et al., 2010; Chaudhury et al., 2014a; Barraso et al., in press).

Mechanistic expressions have also been developed, describing aggregation (Darelius et al., 2005; Poon et al., 2008; Chaudhury et al., 2014b) and breakage (Ramachandran et al., 2009) rates. These expressions account for the effects of material properties, such as surface wetness, density, and yield strength. Since mechanistic expressions are based on particle-scale phenomena, such as individual collisions, they typically include terms for collision rates and particle velocities. This particle-scale information is not inherently known, and may depend on process parameters, equipment geometry, and material properties.

In contrast, discrete element modeling (DEM) is a particle-scale framework that tracks individual particles as they move through space and collide. Developed for soft spheres by Cundall and Strack (1979), this high-fidelity modeling tool provides the detailed particle-scale information that the PBM lacks, such as collision rates and velocity profiles, and is sensitive to process parameters, equipment geometry, and material properties. However, DEM does not inherently account for changes in particle size and other properties resulting from aggregation, breakage, consolidation, and liquid addition.

Because of the complementary advantages and limitations of each framework, efforts have been made to couple PBM and DEM. Ingram and Cameron (2005) discussed alternative multi-scale approaches for this problem, focusing on the information exchanged between the two frameworks and their integration. Most multi-scale studies involve one-directional coupling, where DEM data is collected and used within a PBM. Gant et al. (2006) used DEM to evaluate mechanistic coalescence kernels for use in a PBM, and Bouffard et al. (2012) used DEM results to evaluate a spatial transfer in a compartmental PBM. Goldschmidt et al. (2003) used DEM simulations to solve a PBM, replacing small particles with larger ones as they successfully coalesce. Additionally, Reinhold and Briesen (2012) developed a coupled PBM-DEM model for wet granulation, using DEM simulations to evaluate a mechanistic aggregation rate kernel. Recently, Barraso and Ramachandran (in press) implemented bi-directional coupling between PBM and DEM to evaluate collision frequencies and liquid distribution as a proof-of-concept, and Sen et al. (2014) combined this work with a computational fluid dynamics model to simulate fluidized bed granulation. Further, Barraso et al. (2014) used DEM data to train an artificial neural network, which was then coupled with a PBM to capture collision rates as they depend on the impeller speed, particle size, and size distribution in the system.

In this study, a bi-directional coupling algorithm for PBM and DEM is presented and demonstrated for a twin-screw wet granulation process, developing a hybrid model to predict the effects of material properties, process parameters, and equipment geometry on the CQAs of the product.

1.2. Objectives

In order to predict the CQAs of a granulation process, a mechanistic process model is coupled to a particle-scale model. The purposes of this study are to:

- Present a mechanistic, two-dimensional PBM for a wet granulation process with sensitivities to material properties, process parameters, and particle-scale behavior.
- Develop an efficient bi-directional coupling algorithm, using DEM simulations to provide particle-scale data to the PBM.
- Determine the optimal settings for the model by characterizing the DEM simulation results.
- Apply the model to a twin-screw granulation process and demonstrate the model's sensitivity to equipment geometry, process parameters, and material properties on the CQAs of the product.

This work extends on previous models presented by Barraso and Ramachandran (in press) and Sen et al. (2014), incorporating mechanistic expressions for aggregation, breakage, and consolidation and evaluating these rates using particle velocity and collision data from DEM. Variations in particle properties, such as porosity and liquid content, are also accounted for in DEM simulations using empirical correlations for coefficients of restitution and Young's moduli.

2. Model development

A bi-directionally coupled model was designed to use particle-scale information from DEM simulations within a mechanistic PBM, which tracked changes in the particle size distribution, liquid content, and porosity. The hybrid model captures sensitivities of the product CQAs with respect to material properties, process parameters, and equipment geometries. An overall schematic of the model is presented in Fig. 1. The model was applied to

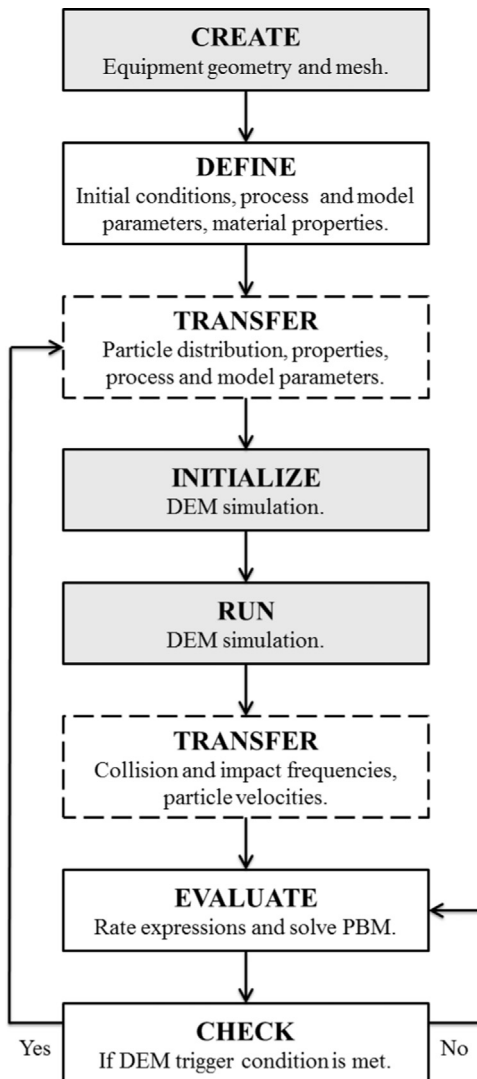


Fig. 1. Schematic of bi-directional coupling approach. Boxes shaded in gray are executed in STAR-CCM+, and white, solid-lined boxes are executed in gPROMS ModelBuilder. Dashed lines indicate data transfer across software platforms. Steps contained within the loop are fully automated, while steps outside the loop require user input.

individual axial compartments in a TSG with no material inflow or outflow, treating the process as a batch system. Future work involves combining several compartments and quantifying flow behavior between them using DEM simulations to create a fully representative model of a continuous TSG.

2.1. Population balance model development

A detailed, two-dimensional PBM was developed and solved using gPROMS ModelBuilder 4.0 (Process Systems Enterprise). The resulting population balance equation (PBE), shown in Eq. (1), tracks particle distributions with respect to size and liquid volume as the particles undergo aggregation, breakage, consolidation, and liquid addition. Nucleation and layering were omitted from this study to focus on the later stages of granulation after nuclei have formed. In future work, these subprocesses will be incorporated into this framework.

$$\frac{\partial F}{\partial t} + \frac{\partial}{\partial V} \left(F \frac{dV}{dt} \right) + \frac{\partial}{\partial V_L} \left(F \frac{dV_L}{dt} \right) = \mathfrak{R}_{agg} + \mathfrak{R}_{break}$$

$$F = F(V, V_L, t) \quad (1)$$

The particle volume is given by V , and the volume of liquid contained within or on the surface of the particle is given by V_L . The number of particles in each size and liquid class is given by F . The convective terms represent the change in the number of particles in each class due to consolidation and liquid addition, as the particles experience property changes and move throughout the 2-D grid. The aggregation and breakage source terms are given by \mathfrak{R}_{agg} and \mathfrak{R}_{break} .

In order to track the porosity of each class, the lumped parameter approach was used, assuming that all particles of the same size and wetness have the same porosity (Barrasso and Ramachandran, 2012; Barrasso et al., 2013). The resulting PBE is given in Eq. (2), where V_S is the volume of solid, per particle, in each class.

$$\frac{\partial FV_S}{\partial t} + \frac{\partial}{\partial V} \left(FV_S \frac{dV}{dt} \right) + \frac{\partial}{\partial V_L} \left(FV_S \frac{dV_L}{dt} \right) = \mathfrak{R}_{S,agg} + \mathfrak{R}_{S,break}$$

$$V_S = V_S(V, V_L, t) \quad (2)$$

The remainder of the volume is occupied by pores. Here, the convective terms account for the transfer of solid as particles move along the grid due to consolidation and liquid addition. $\mathfrak{R}_{S,agg}$ and $\mathfrak{R}_{S,break}$ track the rates of change in the total solid volume in each class due to aggregation and breakage.

These four rate processes can strongly influence the CQAs of the product. Aggregation and breakage result in particle size changes, affecting the product size distribution. Further, the amount of liquid on the surface of the particles affects the rate at which aggregation occurs, so the amount and distribution of liquid binder influences the product size distribution. The consolidation rate determines the porosity of the product granules, affecting the strength and compatibility of the product granules. Additionally, the porosity will influence the breakage rate, as weaker particles break more easily, and the aggregation rate, as a decrease in porosity results in more liquid available on the surface of particles.

Using the 2-D PBM with the lumped parameter of pore volume, three particle properties are tracked: particle volume, liquid volume, and solid volume. From these three attributes, additional properties are evaluated. The volume of liquid associated with each particle was considered to be independent of the total volume, assuming that the liquid either occupies pore space or remains on the surface, outside of the particle. The total volume of the particle is composed of the solid volume and the pore volume (V_p), given by Eq. (3). Assuming that all particles in the system are spherical, the particle diameter can be calculated based on the particle volume, or the first internal coordinate in the PBM (Eq. (4)).

As shown in Eq. (5), the porosity (ϵ) is the ratio of the pore volume to particle volume.

$$V = V_S + V_p \quad (3)$$

$$d = \left(\frac{6V}{\pi} \right)^{1/3} \quad (4)$$

$$\epsilon = \frac{V_p}{V} \quad (5)$$

The aggregation rate is strongly affected by the amount of liquid on the surface of particles (Ennis et al., 1991; Iveson et al., 2001). To capture this effect, a distinction is made between internal ($V_{L,int}$) and external ($V_{L,ext}$) liquid, as shown in Eqs. (6) and (7).

$$V_L = V_{L,int} + V_{L,ext} \quad (6)$$

$$V_{L,int} = \min(V_L, s^* V_p) \quad (7)$$

Liquid is assumed to penetrate the pore space instantly until a maximum fraction of the pore volume, given by s^* , is filled

Table 1
Values of input parameters representing the base case.

Parameter	Type	Value
Liquid-to-solid ratio ($L : S$)	Process parameter	0.25
End of liquid addition ($t_{liquid,stop}$)	Process parameter	15 s
Batch time (t_{batch})	Process parameter	30 s
Screw speed	Process parameter	240 RPM
Maximum pore saturation fraction (s^*)	Material property	0.75
Binder viscosity (μ)	Material property	0.05 Pa s
Primary particle size (d_p)	Material property	5 μm
Density of solid and liquid components (ρ_S, ρ_L)	Material property	2000 kg m ⁻³ , 1000 kg m ⁻³
Consolidation rate constant (K_{cons})	Material property	0.005
Surface asperity height (h_a)	Material property	5 μm
Critical Stokes deformation number (St_{def}^*)	Material property	0.2
Coefficient of restitution slope, intercept (e_{slope}, e_0)	Material property	0.5, 0.5
Poisson's ratio	Material property	0.2
Ratio of Young's modulus to yield strength	Material property	162
Particle-particle coefficients of static, rolling friction	Material property	0.35, 0.2
Particle-wall coefficients of static, rolling friction	Material property	0.16, 0.2
Initial median diameter (d_{50})	Initial condition	0.75 mm
Initial standard deviation of particle size	Initial condition	0.2 mm
Initial volume charge	Initial condition	1500 mm ³
Initial porosity	Initial condition	0.6
Number of grid points in each dimension (N, N_L)	Model setting	9, 10
DEM settling, simulation times ($\Delta t_{settle}, \Delta t_{DEM}$)	Model setting	0.1 s, 0.25 s
Trigger condition: absolute change in L:S ratio	Model setting	0.05
Trigger condition: relative change in $d_{4.3}$	Model setting	10%
Implicit unsteady solver time step	Model setting	1e-4 s
Screw section length	Equipment geometry	16 mm
Screw diameter	Equipment geometry	16 mm

(Chaudhury et al., 2014b). Any additional liquid remains on the surface and contributes to aggregation. The value of s^* is presented in Table 1.

As shown in Eqs. (8) and (9), the wet (m_{wet}) and dry (m_{dry}) masses of each particle can be calculated based on the densities of the solid and liquid components, ρ_S and ρ_L , assuming vacant pore space has negligible mass.

$$m_{wet} = V_S \rho_S + V_L \rho_L \quad (8)$$

$$m_{dry} = V_S \rho_S \quad (9)$$

The values for ρ_S and ρ_L are listed in Table 1.

Assuming that liquid is distributed evenly with respect to particle volume, the rate of liquid addition, per particle, is given by Eq. (10).

$$\frac{dV_L}{dt} = \frac{\dot{V}_{in} V}{V_{total}} \quad (10)$$

\dot{V}_{in} is the total volumetric rate of liquid addition to the system and V_{total} is the total volume of particles in the system. Liquid was added between $t=0$ s and $t=t_{liquid,stop}$. During this period, the total liquid addition rate is given by the following equation.

$$\dot{V}_{in} = \frac{(L : S)V_{S,total}}{t_{liquid,stop}} \quad (11)$$

$V_{S,total}$ is the total volume of solid in the system, and $L : S$ is the overall liquid-to-solid ratio. The values of these parameters are listed in Table 1.

As porous particles collide and deform, their porosity decreases, resulting in smaller, denser granules with a greater amount of surface liquid. The consolidation rate expression used in this study is based on that presented by Ennis et al. (1991) and Tardos et al. (1997), in which the degree of consolidation for a single collision depends on the viscous or deformation Stokes number. Based on this theory, the rate of change in the volume of

a particle is given by the following equation.

$$\frac{dV}{dt} = -K_{cons} V C_{impact} (1 - \exp(-St_{def})) \quad (12)$$

K_{cons} is a rate constant representing the fraction of pore space affected by a single collision, given in Table 1. The impact rate, in collisions per particle per second, is given by C_{impact} . The value for C_{impact} was evaluated using DEM to capture dependencies on the particle properties, equipment geometry, and process parameters, including particle-particle and particle-wall/screw collisions. It should be noted that particle-wall/screw collisions accounted for approximately 40% of all impacts for the base case in DEM simulations. St_{def} is Stokes deformation number, given by the following equation.

$$St_{def} = \frac{\rho_S U_0^2}{2\tau_y} \quad (13)$$

U_0 is the particle velocity, and τ_y is the yield strength (Tardos et al., 1997; Iveson et al., 2001). The average particle velocity for each size and liquid class was obtained using DEM simulations, and the dynamic yield strength was approximated based on the porosity using Eq. (14), where μ is the binder viscosity and d_p is the diameter of the primary particles, given in Table 1 (van den Dries and Vromans, 2002).

$$\tau_y = \frac{9(1-\epsilon)^2 9\mu U_0}{8\epsilon^2 16d_p} \quad (14)$$

Aggregation is a primary mechanism of particle growth in wet granulation processes. Collisions between wet particles can result in coalescence, effectively replacing two small particles with one larger particle. As shown in Eq. (15), the net aggregation rate of a particular class is equal to the difference between the rates of formation ($\mathfrak{R}_{agg,form}$) and depletion ($\mathfrak{R}_{agg,dep}$) (Immanuel and Doyle, 2005; Barraso and Ramachandran, 2012).

$$\mathfrak{R}_{agg}(V, V_L, t) = \mathfrak{R}_{agg,form}(V, V_L, t) - \mathfrak{R}_{agg,dep}(V, V_L, t)$$

$$= \frac{1}{2} \int_0^V \int_0^{V_L} \beta(V - V', V_L - V'_L, V, V'_L, t) F(V - V', V_L - V'_L, t) F(V', V'_L, t) dV'_L dV' \\ - \int_0^\infty \int_0^\infty \beta(V, V_L, V', V'_L, t) F(V, V_L, t) F(V', V'_L, t) dV'_L dV' \quad (15)$$

The aggregation rate kernel, $\beta(V, V_L, V', V'_L, t)$, describes the rate at which two particles in classes V, V_L and V', V'_L coalesce. Because the rate kernel can depend on particle porosity, which is tracked as a lumped parameter, its value can change over time as the particles consolidate. The aggregation rate kernel can be thought of as the product of the frequency of collisions between the two classes $C_{\text{collision}}$ and the probability that a collision will result in coalescence Ψ , as shown in Eq. (16) (Gantt et al., 2006; Barrasso and Ramachandran, in press).

$$\beta(V, V_L, V', V'_L, t) = C_{\text{collision}}(V, V', t) \Psi(V, V_L, V', V'_L, t) \quad (16)$$

The collision frequency was evaluated on a per-particle basis using DEM simulations, which reported the number of collisions between any two size classes. For the purposes of this study, it was assumed that the collision frequency is independent of liquid content, and all collisions between two size classes were counted equally regardless of their liquid classes.

The collision efficiency was estimated based on the Stokes criterion for Type I coalescence, which states that a collision is successful if the viscous Stokes number associated with the collision, St_v , is less than the critical Stokes number of the particles, St_v^* , given by the following equations (Iveson et al., 2001).

$$St_v = \frac{8\tilde{m}U}{3\pi\tilde{d}^2\mu} \quad (17)$$

$$St_v^* = \left(1 + \frac{1}{e}\right) \log\left(\frac{h}{h_a}\right) \quad (18)$$

The harmonic mean masses and diameters of the two particles are given by \tilde{m} and \tilde{d} , and the collision velocity is given by U . e is the coefficient of restitution, h is the thickness of the liquid on the surface of the particle, equal to $dV_{\text{ext}}/6V$, and h_a is the height of the surface asperities, given in Table 1 (Liu et al., 2000). Based on this criterion, a critical velocity, U_{crit} can be determined below which all collisions result in coalescence, as shown in the following equation

$$U_{\text{crit}} = \left(1 + \frac{1}{e}\right) \log\left(\frac{h}{h_a}\right) \frac{3\pi\tilde{d}^2\mu}{8\tilde{m}} \quad (19)$$

The collision efficiency was evaluated from a collision velocity distribution, $p(U)$, as presented in the following equation.

$$\Psi = \int_0^{U_{\text{crit}}} p(U) dU \quad (20)$$

Based on an examination of DEM results, the collision velocity distribution between any two particle classes was assumed to obey a log-normal distribution, shown in Eq. (21), where U_0 and sd_U are the mean and standard deviation of the velocity, respectively.

$$p(U) = \frac{1}{U\sqrt{2\pi\sigma}} \exp\left[-\frac{(\ln U - \mu)^2}{2\sigma^2}\right] \quad (21)$$

$$U_0 = e^{\mu - \sigma^2/2} \quad (22)$$

$$sd_U^2 = (e^{\sigma^2} - 1)e^{2\mu + \sigma^2} \quad (23)$$

The mean and standard deviation of the collision velocity for any two classes were assumed to be equal to the average values of the particles in those classes. The particle velocities for each class and their standard deviations were obtained from DEM simulations.

Similarly, the net breakage rate was evaluated for each class from the formation and depletion terms, as shown in the following equation.

$$\mathfrak{R}_{\text{break}}(V, V_L, t) = \mathfrak{R}_{\text{break,form}}(V, V_L, t) - \mathfrak{R}_{\text{break,dep}}(V, V_L, t) \\ = \int_V^\infty \int_{V_L}^\infty b(V', V'_L, V, V_L) K_{\text{break}}(V', V'_L, t) \\ \times F(V', V'_L, t) dV' dV'_L - K_{\text{break}}(V, V_L, t) F(V, V_L, t) \quad (24)$$

The rate of breakage, per particle, in each class is given by $K_{\text{break}}(V, V_L, t)$, and the number of fragment particles forming into class V, V_L from a single breakage event of V', V'_L is given by $b(V', V'_L, V, V_L)$.

A simple breakage distribution function was assumed, stating that all breakage events result in two particles of equal size and liquid volume, as presented in the following equation.

$$b\left(V', V'_L, \frac{V'}{2}, \frac{V'_L}{2}\right) = 2 \quad (25)$$

For all other values of V and V_L , $b=0$.

The breakage rate kernel was evaluated based on a Stokes criterion, where an impact will result in breakage if the associated Stokes deformation number is greater than a critical Stokes deformation number, St_{def}^* (Tardos et al., 1997; Iveson et al., 2001). By combining this criterion with Eqs. (13) and (14) and solving for the velocity, a critical breakage velocity (U_{break}) is determined, above which breakage will occur, as shown in the following equation.

$$U_{\text{break}} = \frac{2St_{\text{def}}^*}{\rho_S} \frac{9(1-\epsilon)^2}{8} \frac{9\mu}{\epsilon^2} \frac{16d_p}{16d_p} \quad (26)$$

Various values for St_{def}^* have been reported in the literature, ranging from 0.01 to 0.2 (van den Dries and Vromans, 2002; Liu et al., 2009; Smith et al., 2010). The value used in this study is listed in Table 1.

As with aggregation, a log-normal impact velocity was assumed based on the average particle velocity of each class obtained from DEM simulations. Shown in Eq. (27), the breakage kernel is equal to the product of the impact rate and the fraction of those impacts resulting in breakage, evaluated from the velocity distribution function.

$$K_{\text{break}} = C_{\text{impact}} \int_{U_{\text{break}}}^\infty p(U) dU \quad (27)$$

The initial particle size distribution was assumed to follow a log-normal mass distribution, with a fixed median diameter (d_{50}), standard deviation, and total volume. These values, along with the initial porosity, are listed in Table 1. All particles were assumed to be dry initially, with negligible liquid volume.

To solve this PBM, the two internal coordinates were discretized to form a 2D grid. The volume coordinate was discretized into N classes, with the diameter (in mm) of each class i defined in Eq. (28). The liquid volume coordinate was divided into N_L classes, where the smallest class represents negligible liquid volume, and the remaining classes have liquid volumes equal to those of the volume grid. Finite difference methods were used to evaluate the convective terms for consolidation and liquid addition on the discretized grid. The aggregation and breakage source terms were evaluated using the cell average technique (Chaudhury et al., 2013; Barrasso and Ramachandran, 2012). The resulting system of algebraic and ordinary differential equations were solved using the differential-algebraic numerical solvers in gPROMS, which uses a backwards differentiation formula for dynamic integration. The values for N and N_L are provided in Table 1.

$$d(i) = 0.5 \exp\left(\frac{i-1}{4}\right) \text{mm} \quad (28)$$

Throughout this PBM, mechanistic rate expressions call for additional data to describe particle velocity and collision behavior. For example, the particle velocity distribution affects the aggregation, breakage, and consolidation rates. At greater velocities, breakage and consolidation occur, while aggregation is favored at lower velocities. Additionally, the rates of collisions between any two particle sizes influence their aggregation rates, and the impact frequency is used in breakage and consolidation rate expressions. The values for these parameters may depend on equipment geometry (screw element configuration, impeller design), material properties (density, coefficient of restitution), process parameters (screw/impeller speed), and the state of the system (size distribution, liquid fraction). To evaluate this particle-scale behavior, the PBM is coupled with DEM simulations.

2.2. Discrete element method simulations

DEM simulations were performed using STAR-CCM+ v9.02 (CD-adapco). A 3D CAD model was created in STAR-CCM+ for an axial section of a twin-screw granulator based on the EuroLab 16 mm TSG (Thermo Fisher Scientific). The length of the section and the screw diameter are listed in Table 1. As shown in Fig. 2, two screw element types were modeled: a block of mixing elements and a feed screw. The screws were rotated at a fixed speed, and a sliding interface was created to resolve the boundary between the screw space and the wall. A periodic interface was created from the axial boundaries of the TSG section to allow particles that exit the section to enter from the other side. This geometry was meshed using the polyhedral mesher and embedded thin mesher models in STAR-CCM+, resulting in approximately 40,000 volume cells to capture the geometric details of the equipment. The implicit unsteady solver was used with a fixed time step, as given in Table 1, and the DEM solver uses a variable time step to sub-step the simulation as the particles move, balancing accuracy, stability, and computational expense.

Spherical particles were created to represent each of the classes in the PBM, specifying the properties of size, density, Young's modulus, and Poisson's ratio. The size and density are provided directly by the PBM. The Young's modulus was estimated based on the yield strength for each class Eq. (14). A constant ratio of the Young's modulus to yield stress was assumed, using the value presented by Hassanpour and Ghadiri (2004) for lactose. The Poisson's ratio was assumed to be constant and equal for all particle types. The values for these parameters are presented in Table 1.

The Hertz-Mindlin contact model was used as implemented in STAR-CCM+ to resolve particle-particle and particle-wall collisions based on three interaction coefficients: restitution, static friction, and rolling friction (CD-adapco, 2014). The coefficient of restitution (e) is a measure of the ratio of rebound to impact

velocities and has been shown to depend on the liquid content of the particles at low velocities (Iveson and Litster, 1998; Mangwandi et al., 2007). A linear dependence on liquid content was assumed, as shown in Eq. (29), where e_0 and e_{slope} are the intercept and slope of the coefficient of restitution, respectively.

$$e = e_0 - e_{slope} \frac{L_{ext}}{L_{ext} + V} \quad (29)$$

For particle-particle collisions, this equation is evaluated based on the average external liquid fraction of the two particle types. Constant and equal coefficients of static and rolling friction were used, and their values were chosen based on those used by Hassanpour and Ghadiri (2004) and Ai et al. (2011), as presented in Table 1.

Four pieces of information are obtained from the DEM simulations and used within the PBM: the average (U_0) and standard deviation (s_U) of the particle velocity for each size/liquid class, the impact frequency (C_{impact}) of each particle size class, and the collision frequency ($C_{collision}$) between any two particle size classes. The collision and impact frequencies are reported on a per-particle and per-second basis, as determined from the following equations.

$$C_{impact}(i) = \frac{N_{impact}(i)}{F(i)\Delta t_{DEM}} \quad (30)$$

$$C_{collision}(i,j) = \frac{N_{collision}(i,j)}{F(i)F(j)\Delta t_{DEM}} \quad (31)$$

$N_{impact}(i)$ is the number of collisions between particles of size class i and any other particles or the wall during the time interval Δt_{DEM} . $N_{collision}(i,j)$ is the number of collisions between particles of size classes i and j (Gantt et al., 2006; Barraso and Ramachandran, in press). Here, $F(i)$ represents the total number of particles in size class i , regardless of liquid content.

The number of collisions between any pair of particle types (or the wall) is estimated based on the trajectory of their number of contacts over time. If the number of contacts increases over a time step, the additional contacts are considered new collisions and are added to a running total. If the number of contacts decreases or stays constant, it is assumed that no new collisions occur over that time step. The number of impacts is calculated from the collision data. To evaluate the particle velocity, the mean and standard deviation of the particle velocity for each class are tracked over time, and the average values during the interval are calculated from these trajectories.

It must be noted that if there are no particles present in a particular class, the DEM simulation has no data for that class to provide to the PBM. As particles form in these classes, reasonable approximations are used in place of missing data until the next DEM simulation is performed. The maximum collision and impact frequencies are used for any empty classes, since those classes are typically the largest particles, which collide more frequently. The

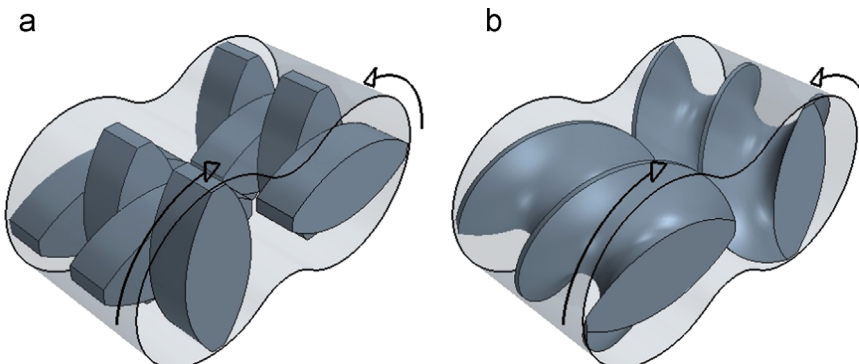


Fig. 2. 3D CAD models of axial section of a twin-screw granulator with (a) feed screw elements and (b) mixing elements. Arrows indicate direction of screw rotation.

mean and standard deviation of the velocity for all particles is used for the empty classes.

The previously described particle properties and interaction coefficients can have a profound impact on particle and collision scale behavior. Freireich et al. (2009) found that both the collision frequency and impact velocity distributions are sensitive to the coefficient of restitution and the particle stiffness. At greater stiffnesses, collisions occur more frequently and at lower velocities. This observation suggests that stiffer particles will aggregate at a greater rate than less stiff particles, since they will collide more often and with a greater efficiency.

Freireich et al. (2009) also found that the coefficient of restitution affects the collision frequency and velocity distribution. At greater coefficients of restitution, collision frequencies and impact velocities are increased, resulting in more breakage and consolidation. Although the collision frequency is increased, aggregation rates are reduced because the average velocities increases and the critical velocities decreases.

2.3. Bi-directional coupling of PBM and DEM

As particles take up liquid, aggregate, and consolidate, their properties change, and the particle-scale behavior is affected. To account for these changes, a bi-directional coupling algorithm was developed, combining particle-scale information from DEM with the process-scale PBM. The PBM tracks changes in particle size distributions and properties, and DEM simulations are performed when significant changes are observed to obtain new collision and velocity data. DEM is more computationally expensive than PBM, and limiting the use of DEM can drastically reduce the computation time. By triggering DEM simulations intermittently, a fraction of the process time is required to obtain meaningful information to use within the PBM. To implement this strategy, all results from the DEM simulations are reported as rates per particle so they can be used in the PBM as the system changes.

A schematic of this coupling algorithm is shown in Fig. 1. Prior to the start of the simulation, the equipment geometry is created and meshed in STAR-CCM+. Values for all material properties, process parameters, initial conditions, and model settings are defined in gPROMS. The simulation is then executed from the gPROMS user interface, and the bi-directional coupling algorithm is implemented automatically. A DEM simulation must be performed initially to obtain values for the collision and velocity data.

The gPROMS Foreign Process Interface (FPI) was used to transfer information to STAR-CCM+, execute DEM simulations, and import DEM results into the PBM. A custom FPI was written using C++ to accomplish these tasks. First, the FPI writes the process parameters, particle distributions, material properties, and model settings to files. A summary of the data transferred across the two software platforms is presented in Table 2.

The FPI then executes a command to run a simulation in STAR-CCM+ using a custom Java macro. From the Java macro, the files created by the FPI are read and necessary changes are made to the STAR-CCM+ simulation. Process parameters (e.g. screw speed) and model settings (e.g. Δt_{settle} , Δt_{DEM}) are adjusted. A particle type is created for each class that contains one or more particles and values for the material properties are set. Interactions are defined between each pair of particle classes and between each class and the equipment, defining the values for the coefficients of restitution and friction for each interaction.

Particles are inserted at random locations in the equipment to achieve the particle distribution specified by the PBM, rounding to the nearest whole numbers as needed, and the DEM simulation runs for a brief interval to allow particles to settle. After the particles settle, monitors are created to track the number of contacts between each pair of particles and the average velocity

Table 2

Data exchanged between gPROMS and STAR-CCM+.

gPROMS to STAR-CCM+	
Number of classes in each dimension (N, N_L)	
Number of particles in each class (F)	
Diameter (d), density (ρ), Young's modulus and Poisson's ratio of each class	
Coefficients of restitution (e), static friction, and rolling friction for each pair of classes, wall	
DEM time intervals for settling, simulation ($\Delta t_{\text{settle}}, \Delta t_{\text{DEM}}$)	
Screw speed	
STAR-CCM+ to gPROMS	
Average particle velocity of each size/liquid class (U_0)	
Standard deviation of the particle velocity of each size/liquid class (sdu_U)	
Collision frequency of each pair of size classes ($C_{\text{collision}}$)	
Impact frequency of each size class (C_{impact})	

of each particle type. Finally, the full DEM simulation is executed, and results are processed to export collision frequencies, impact rates, and average velocities. These values are written to a file to be read by gPROMS.

After the DEM simulation is complete, the FPI reads the results file and updates the values for collision and velocity data in the PBM. The PBM is then solved until a significant change in the system is observed. When this criterion is met, the PBM pauses and the FPI is executed to run a new DEM simulation and obtain new values for these parameters. This cycle continues until the desired batch time is reached.

Trigger criteria were set to require updated DEM simulations when a significant change is observed in the PBM results. These criteria are met if either the absolute change in the total liquid fraction in the system or the relative change in the volume-average diameter ($d_{4,3}$) exceeds a set value. The values for these trigger conditions are presented in Table 1, and further discussion on the selection of these values can be found in Sections 3.1 and 3.2.

All simulations presented in this study were performed using eight CPUs on an Intel Xeon E5-2687W, 3.1 GHz processor with 128 GB of RAM.

3. Results and discussion

3.1. Characterizing the DEM simulations

Because DEM is much more computationally intensive than the PBM, it is advantageous to limit the DEM simulations while maintaining accuracy by adjusting the frequency with which the DEM simulations are called from the PBM and the amount of time simulated during iteration. DEM simulations were performed independently from the PBM to select these values.

At the start of each iteration, the particles are inserted randomly and allowed to settle for Δt_{settle} before results are collected over an interval of Δt_{DEM} . A DEM simulation was performed using the initial distribution of the base case in the mixing element geometry. Fig. 3 shows trajectories of the average and standard deviation of the particle velocity and number of contacts over time for particles of 1 mm in diameter. Dry particles of various sizes are randomly inserted into the system, with a median diameter of 1.5 mm and a standard deviation of 0.5 mm. All other parameter values are based on the base values presented in Table 1. The mixing element is initially stationary and begins to rotate at 0.05 s. The values of the critical DEM results stabilize after 0.1 s and fluctuate mildly thereafter. Based on these results, values of 0.1 s and 0.25 s were chosen for Δt_{settle} and Δt_{DEM} , respectively, collecting data from one full screw revolution.

To determine the appropriate trigger criteria, an understanding must be developed relating the particle size and property distributions to the outcomes from DEM. Simulations were performed to demonstrate the effects of particle wetness, porosity, and size distribution on the average particle velocity and collision rate.

As shown in Fig. 4, DEM simulations were performed using the base conditions with four different median diameters to illustrate how the collision and velocity data can change as the system evolves. The impact frequency of small particles increases as the

median diameter increases, while that of the larger particles decreases. The size distribution also has a slight effect on the average particle velocity, which increases with average particle size. These results support the need for bi-directional coupling of PBM and DEM, since the particle-scale data from DEM depends on the state of the system, which changes throughout the process. A replicate simulation was performed for the median diameter of 1.5 mm, demonstrating the reproducibility of the data.

Further, the liquid content and porosity of the particles moderately affects the collision and velocity data, as shown in Fig. 5. DEM simulations were performed for a single size distribution ($d_{50}=1.5$ mm, std. dev.=0.5 mm) for three liquid-to-solid ratios and two porosities. Wetter particles have lower coefficients of restitution than drier particles, leading to a decrease in collision and impact frequencies, particularly for larger particles. No significant effect of wetness on particle velocity was observed. Similarly, a decrease in porosity results in a denser particle with a greater Young's modulus, resulting in slightly greater collision and impact frequencies.

Based on these results, a new DEM simulation was performed when the average diameter in the system, according to the PBM, changes by more than 10%. A change in the liquid content has a small but noticeable effect on the results, so an additional DEM trigger condition was set to run a new DEM simulation if the overall liquid fraction changes by more than 0.05.

Finally, DEM simulations were performed to identify the effects of the equipment geometry and screw speed on the particle-scale behavior, as shown in Fig. 6. The same size distribution was simulated for dry particles using a the mixing elements and the feed screw geometries at two different screw speeds. The mixing

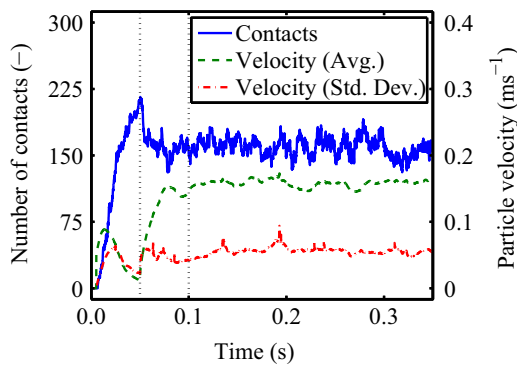


Fig. 3. Time trajectories from DEM simulation showing number of contacts between 1-mm particles with particles of the same size, and the average and standard deviation of the velocity of 1-mm particles. Particles are added at time=0 s with a median diameter of 1.5 mm and a standard deviation of 0.5 mm. Dotted lines indicate start of rotation of the screw and start of data collection, respectively.

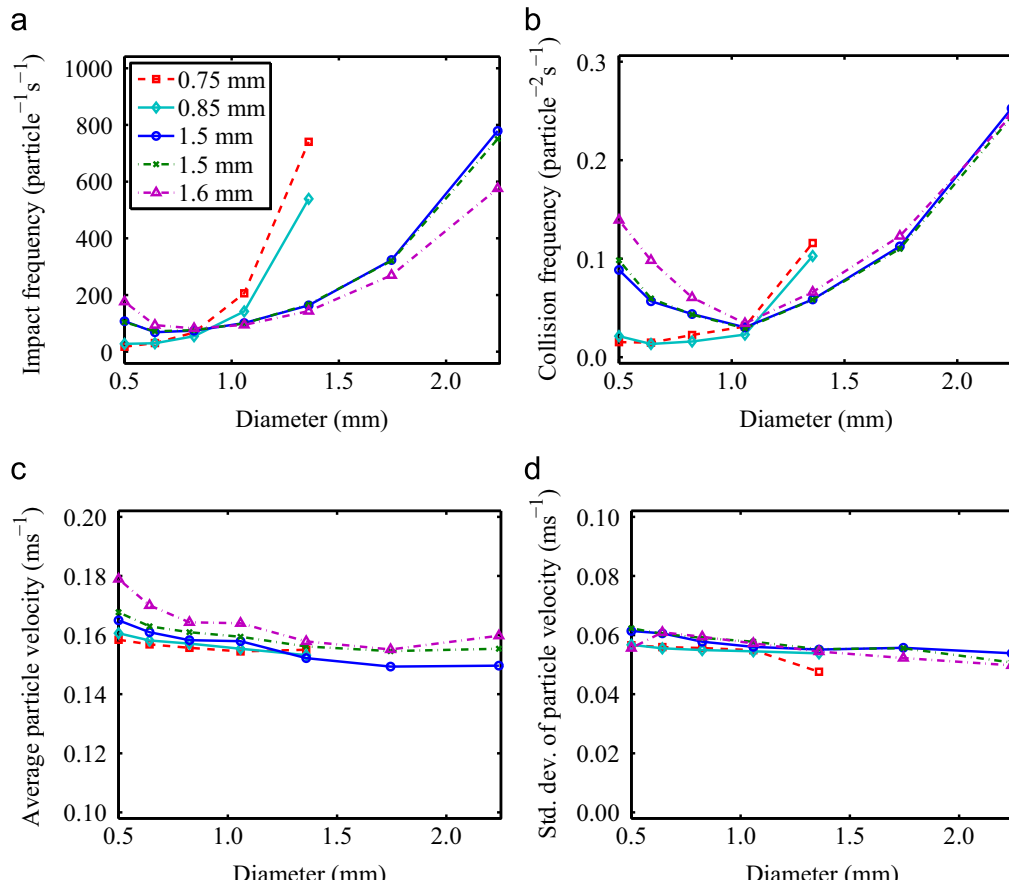


Fig. 4. DEM results showing the effects of size distribution on (a) impact frequency, (b) collision frequency with 1-mm particles, (c) average particle velocity, and (d) standard deviation of particle velocity for each size class. Median diameters are listed in the legend. The standard deviation of the diameter is fixed at 0.2 mm for the smallest two simulations and 0.5 mm for the larger simulations.

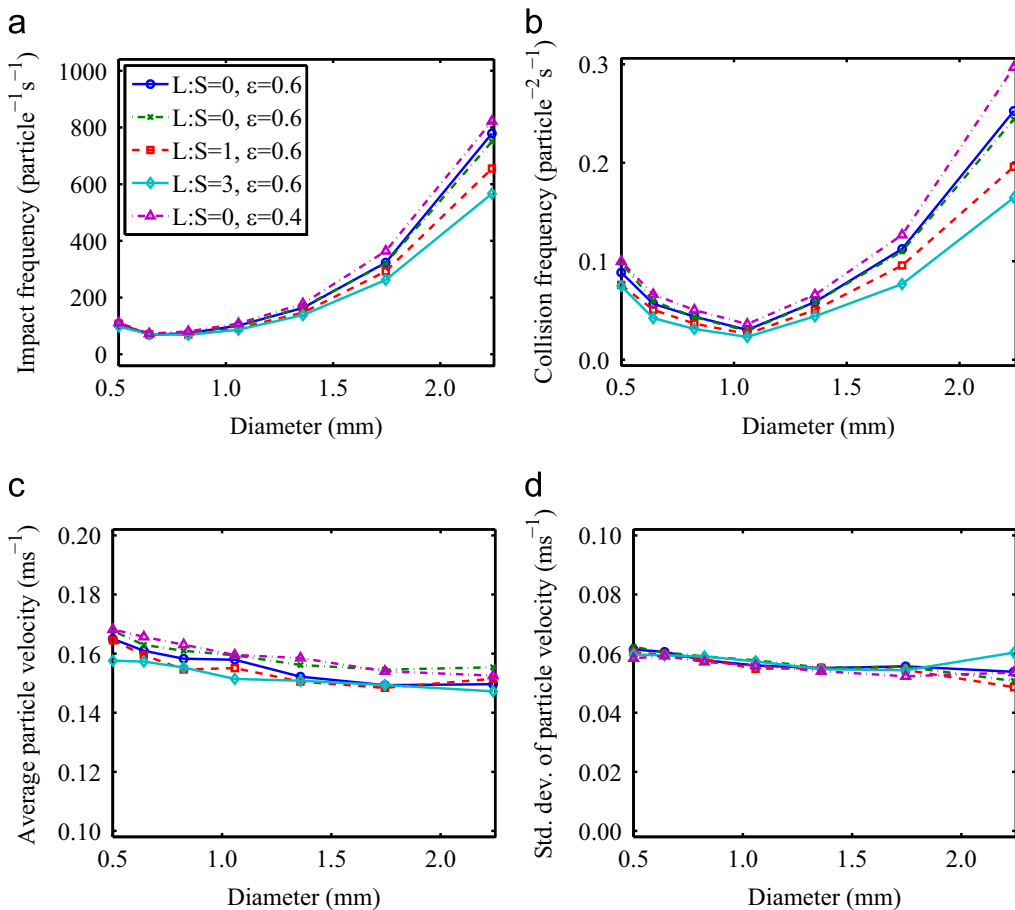


Fig. 5. DEM results showing the effects of particle wetness and porosity on (a) impact frequency, (b) collision frequency with 1-mm particles, (c) average particle velocity, and (d) standard deviation of particle velocity for each size class.

element resulted in greater velocities and collision frequencies than the feed screw as well as a greater variability in the particle velocity. Due to the greater velocities, the mixing element is expected to facilitate more breakage and consolidation than the feed screw. The broader velocity distribution observed in the mixing element may also result in more aggregation since a fraction of the particles are moving slowly enough to coalesce. For both the mixing element and the feed screw, an increased rotational speed results in greater average velocities.

The data obtained from the DEM simulations showed clear sensitivities to the particle properties, process parameters, and equipment geometry. This particle-scale behavior is captured using DEM and transferred to the PBM, forming a predictive model that can identify the effects of these variables on the CQAs of the product.

3.2. PBM-DEM simulations: base case

The results of the coupled PBM-DEM simulations are summarized in Table 3. Two PBM-DEM simulations were performed for the base case in the mixing element geometry. During each simulation, STAR-CCM+ was called 11 times to update the DEM collision and velocity data, resulting in 3.85 s of physical time simulated in DEM. These simulations were solved in 13.1 h. As DEM is more computationally intensive than the PBM, the majority of this time was spent running the DEM simulations. For all coupled simulations, the PBM steps in the simulation were solved in a total of approximately 5 min. By simulating only 3.85 s of the total 30-s process in DEM, the computation time is reduced by approximately 87%. If the computation time scales according to

the DEM simulation time, the full 30-s simulation would take 4.5 days.

Fig. 7(a-c) shows snapshots of the DEM simulations at the beginning, middle, and end of the process. These images show a wide variation in particle velocity as the mixing elements agitate the particles. Additionally, larger granules appear as the particles aggregate and form granules.

In Fig. 8, simulated product size distributions and evolution of the average size, porosity, and total external liquid volume are presented for the base case. Throughout the process, the size distribution widens to include larger particles, while the frequency of small particles increases. This result suggests that aggregation is dominant over breakage. Some small particles remain, either due to a lack of external liquid available for aggregation or breakage and attrition of larger particles. A minimal increase in the average diameter is observed over the first 10 s, but as sufficient liquid is added and the particles consolidate, liquid appears on the surface and aggregation begins to occur. Aggregation continues after the liquid addition period is complete. Initially, the average porosity decreases slowly, but consolidation rates increase as larger granules appear and deform.

Further, the total volume of external liquid increases during the liquid addition period, and decreases as the liquid addition period ends. This observation can be attributed to the aggregation of wet particles with porous dry particles. As a wet particle and a dry particle coalesce, the pore space available for internal liquid increases, and excess liquid enters the pores in the dry particle, reducing the amount of external liquid. The total volume of external liquid then increases due to consolidation, which squeezes the internal liquid onto the surface of the particles.

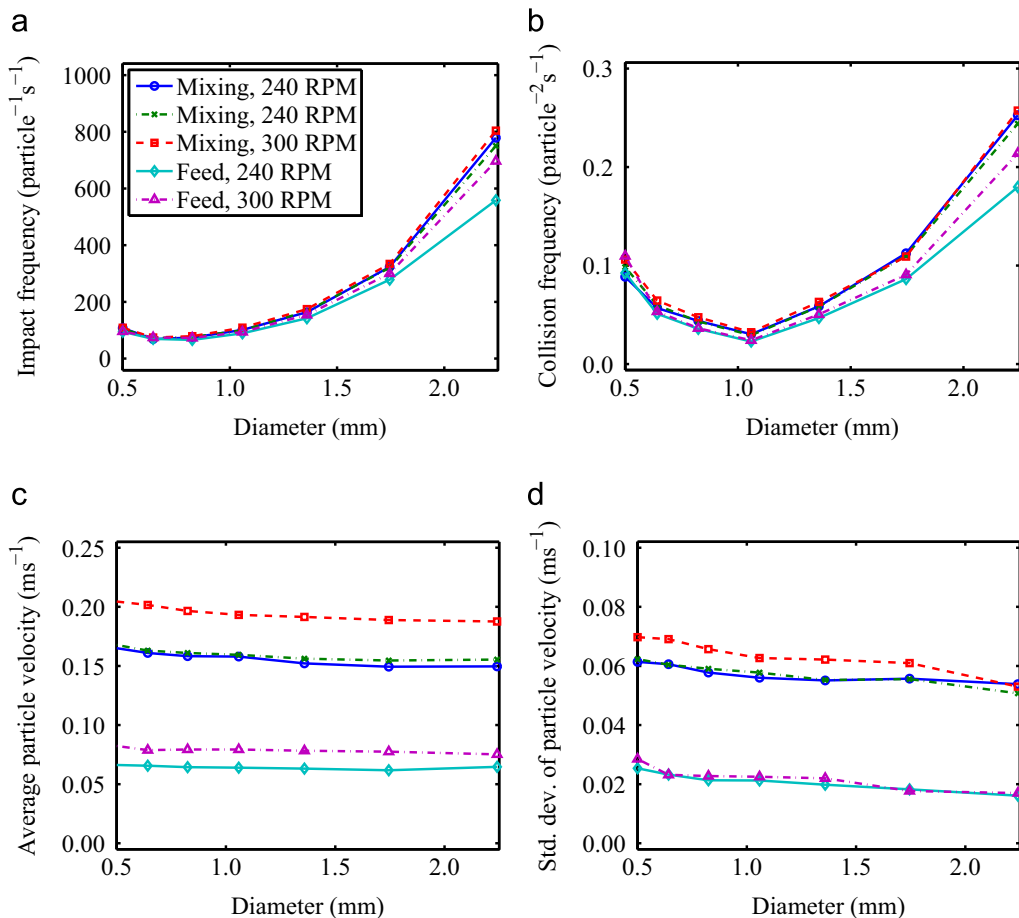


Fig. 6. DEM results showing the effects of screw element type and rotational speed on (a) impact frequency, (b) collision frequency with 1-mm particles, (c) average particle velocity, and (d) standard deviation of particle velocity for each size class.

Table 3
Summary of results of coupled PBM-DEM simulations.

Simulation	DEM iterations	Comp. time (h)	Final $d_{4,3}$ (mm)
1 Base case	11	13.1	1.51
2 Base case replicate	11	13.1	1.57
3 L:S trigger=0.035, $d_{4,3}$ trigger=7%	15	15.4	1.51
4 L:S trigger=0.1, $d_{4,3}$ trigger=15%	6	8.4	1.44
5 300 RPM	11	15.9	1.58
6 Feed screw	7	6.8	0.94
7 Feed screw, 300 RPM	7	7.2	0.99
8 L : S = 0.2	8	7.5	1.19
9 $\mu=0.04$ Pa s	11	13.4	1.61
10 $s^*=0.85$	8	8.9	0.99

Fig. 8 also shows those results for a replicate simulation of the base case and two simulations with modified DEM trigger criteria. The results of the replicate simulation demonstrate reproducibility of the coupled model, suggesting that the DEM iterations contained sufficient numbers of particles and were simulated for a long enough interval to produce reliable data throughout the simulation.

The DEM criteria were tightened to perform DEM simulations when the liquid-to-solid ratio changes by 0.035 or when the average diameter changes by 7%. Under these conditions, 15 DEM iterations were performed throughout the process, resulting in a longer computation time. However, the results are roughly the

same, suggesting that the initial trigger criteria were sufficient to capture the dynamic behavior of the process. Minor differences are observed in the product size distribution in the lower size classes and in the amount of surface liquid shortly after the liquid addition period ends.

Further, the DEM criteria were loosened to trigger a DEM simulation when the liquid-to-solid ratio changes by 0.1 or when the average diameter changes by 15%. The coupled model used 6 DEM iterations and was solved in 8.4 h. Results show a similar evolution in the average velocity and external liquid volume, but a slightly smaller average diameter. This observation suggests that the coupling frequency affects the results, further indicating a need for bi-directional coupling between the two modeling frameworks.

3.3. PBM-DEM simulations: sensitivity analysis

Additional PBM-DEM simulations were performed to assess the model's sensitivity to equipment geometry, process parameters, and material properties. Snapshots of DEM simulations in the mixing element and the feed screw for a rotational speed of 240 RPM are shown in **Fig. 7**.

To evaluate the model's ability to capture realistic trends, the results are compared to two experimental studies that used the co-rotating TSG (16 mm Prism Euro Lab TSG, Thermo Fisher Scientific), similar to the screw element geometries used in DEM simulations. [Dhenge et al. \(2012\)](#) granulated a formulation of α -lactose monohydrate, microcrystalline cellulose, and crosscarmellose sodium using water or a 6% hydroxypropylcellulose solution as

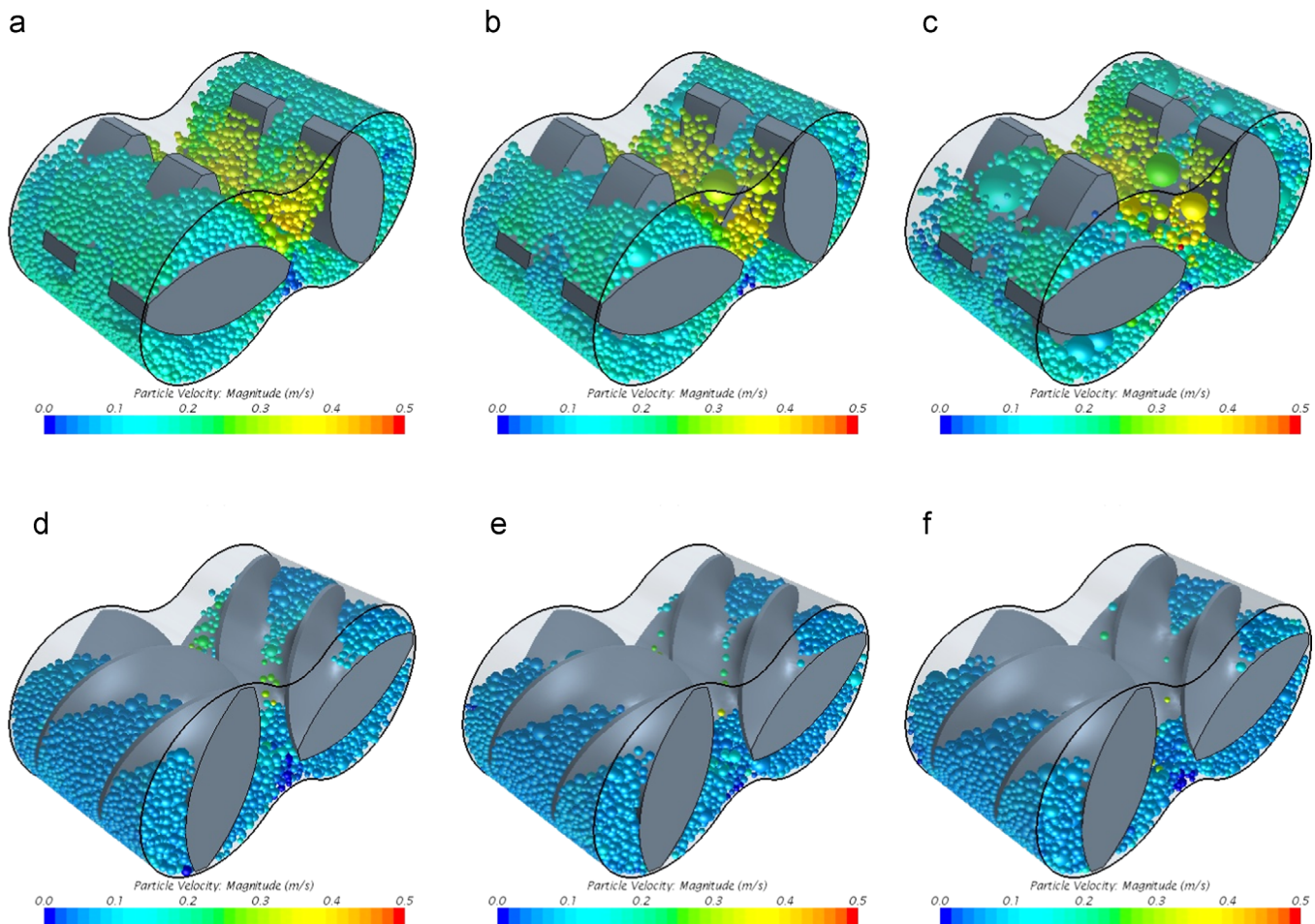


Fig. 7. Snapshots of the DEM simulations for the base case with mixing elements (a–c) and feed screws (d–f) at times of approximately 0, 15, and 30 s, respectively.

the granulating liquid. The screw elements consisted of conveying elements and kneading blocks at a 60° pitch, and the rotation rate of the screw was fixed at 400 RPM. The effects of the liquid-to-solid ratio, binder viscosity, and powder feed rate on the size, strength, and shape of the product granules were observed.

In another study, El Hagrasy et al. (2013) granulated a formulation of α -lactose monohydrate, microcrystalline cellulose, and crosscarmellose sodium using hydroxypropylmethyl cellulose as the binder. The effects of lactose grade, liquid-to-solid ratio, and binder distribution method on the product size distribution and porosity were analyzed, at a constant screw speed of 400 RPM. Screw elements consisted of conveying blocks and kneading elements with a 60° pitch.

From Fig. 7, it is evident that the simulated velocities in the feed screw are lower and more uniform than those in the mixing elements. Fig. 9 shows results for two geometries (mixing elements and feed screws) at two rotational speeds. These results show a strong sensitivity to the equipment geometry. In the feed screw, where velocities and collision rates are reduced, a smaller size change is observed. Little consolidation occurs, resulting in a lower amount of external liquid available for aggregation. Although the particle velocity is lower in the feed screw, favoring aggregation, the critical aggregation velocity is reduced without the presence of surface liquid. The greater degree of consolidation in the mixing elements is consistent with the experimental findings of Dhenge et al. (2012), who determined that the kneading elements promoted consolidation and breakage.

Similarly, the screw speed affected the CQAs of the product in both geometries. At a higher screw speed, more consolidation

occurred, resulting in a greater amount of surface liquid and slightly larger granules. These results demonstrate the sensitivity of the PBM to the results of the DEM simulations. Further, the CQAs of the product, as predicted by the PBM, are affected by changes in the screw speed and the equipment geometry via the DEM simulations. The PBM-DEM model captures these effects, while PBM and DEM by themselves do not, demonstrating the predictive value of the coupled model.

The liquid-to-solid ratio, binder viscosity, and maximum pore saturation fraction were also varied, and their effects on the CQAs were predicted, as shown in Fig. 10. Simulations showed that a decrease in the liquid-to-solid ratio resulted in smaller particles, consistent with the experimental observations of Dhenge et al. (2012) and El Hagrasy et al. (2013), who observed a decrease in the fraction of fine powder particles with an increase in the liquid-to-solid ratio. Since fewer large granules form, less consolidation occurs, further reducing the amount of surface liquid available. The greater porosity observed at the lower liquid-to-solid ratio is consistent with experimental results of El Hagrasy et al. (2013).

An increase in the maximum pore saturation fraction, or the amount of liquid the pores can hold internally, resulted in much smaller granules due to a reduction in the surface liquid. Further research is needed to characterize this material property for a particular powder as an input to the model.

Finally, a reduction in the binder viscosity produced larger granules of a lower porosity. While the aggregation rate increases with viscosity, the consolidation rate decreases due to an increase in granule strength. Because of the additional consolidation that occurs at the lower viscosity, a greater amount of surface liquid is

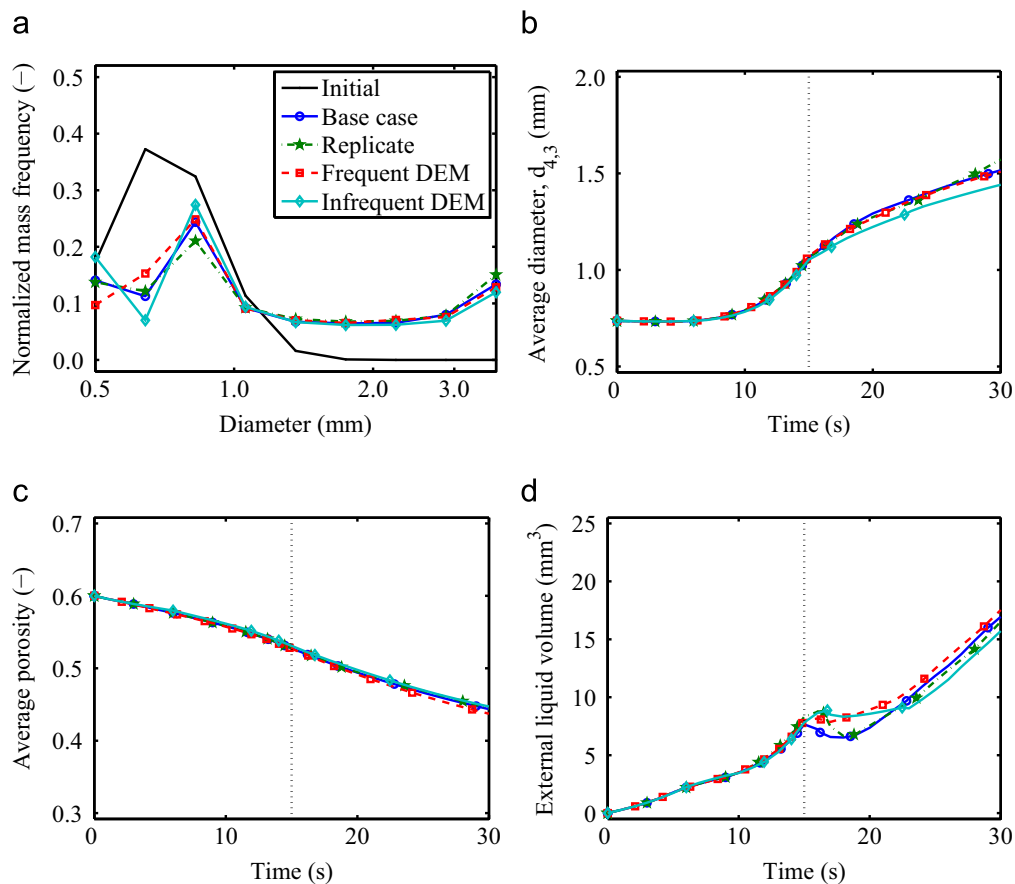


Fig. 8. PBM-DEM results for the base case and a replicate simulation showing (a) the product size distribution, (b) the average diameter over time, (c) the average porosity over time, and (d) the total volume of external liquid over time. The points on time plots indicate DEM iterations. Vertical lines denote the end of the liquid addition period.

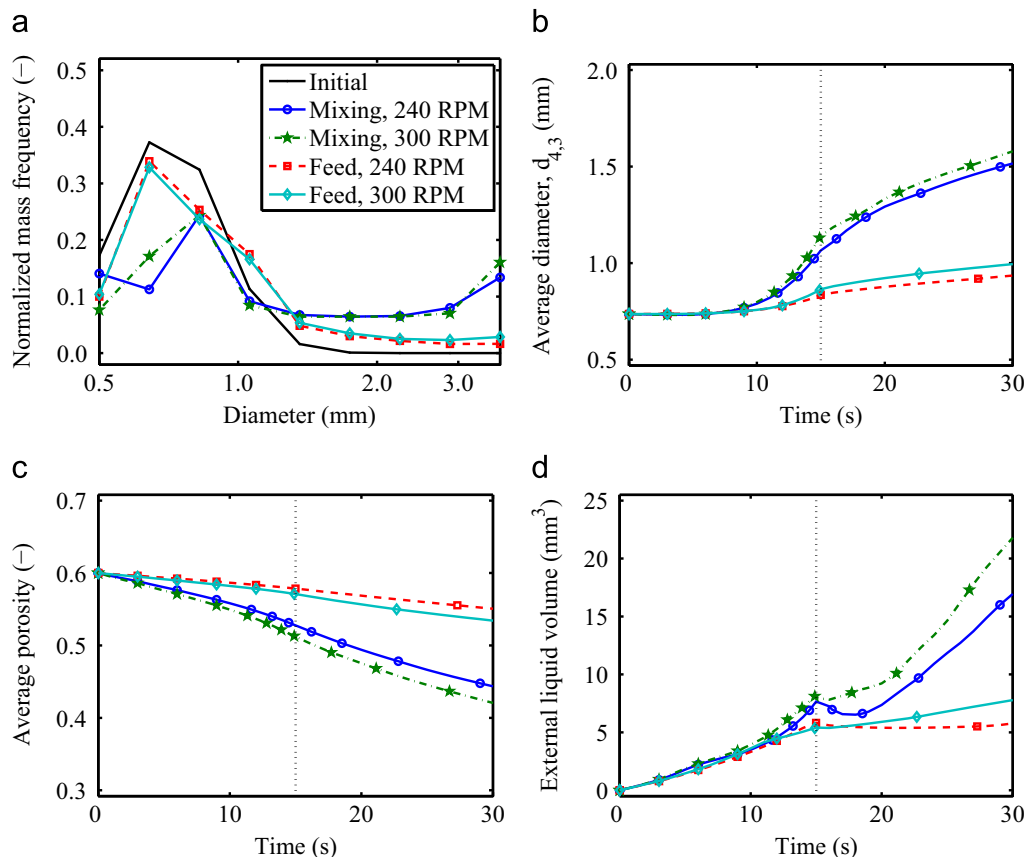


Fig. 9. PBM-DEM results showing effects of equipment geometry and screw speed on (a) the product size distribution, (b) the average diameter over time, (c) the average porosity over time, and (d) the total volume of external liquid over time. The points on time plots indicate DEM iterations. Vertical lines denote the end of the liquid addition period.

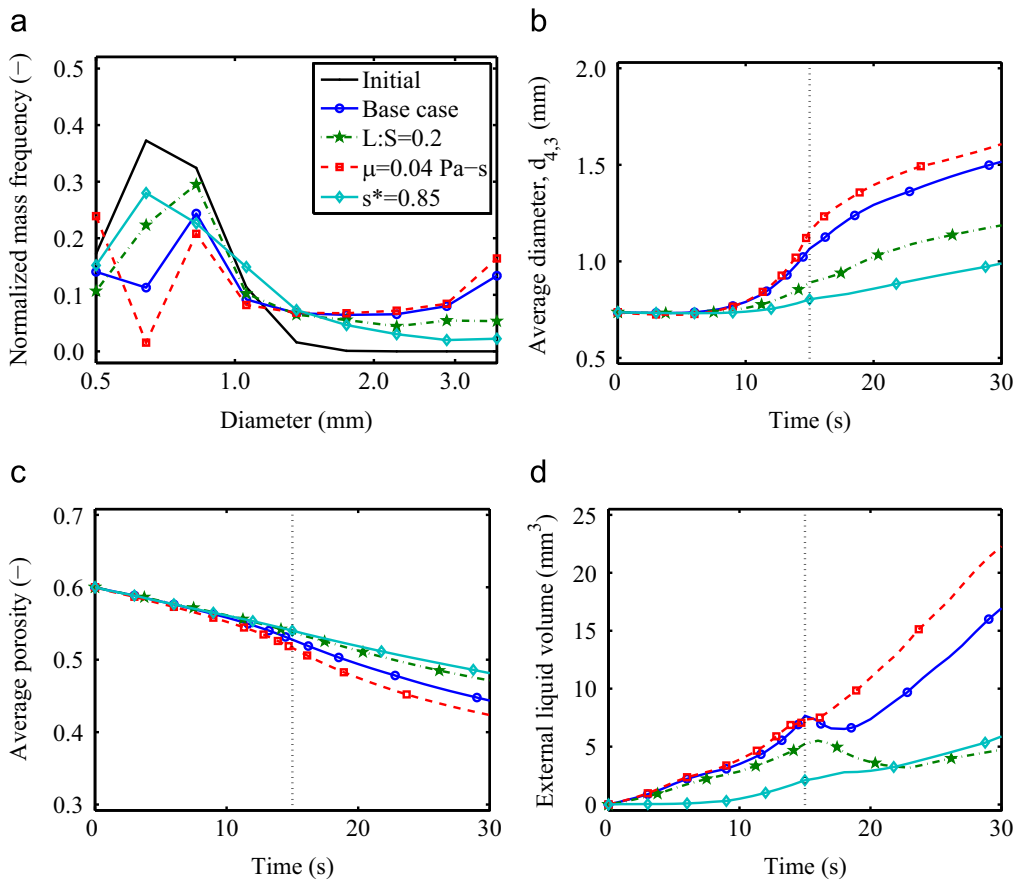


Fig. 10. PBM-DEM results showing effects of the liquid-to-solid ratio, binder viscosity, and maximum pore saturation fraction on (a) the product size distribution, (b) the average diameter over time, (c) the average porosity over time, and (d) the total volume of external liquid over time. The points on time plots indicate DEM iterations. Vertical lines denote the end of the liquid addition period.

available, and larger granules are formed. The effects of binder viscosity on the aggregation and consolidation rates are competing, and the direction of these trends may depend on other factors, such as the total amount of liquid in the system. In addition, an increase in the amount of small particles is also observed at the lower viscosity, resulting in a bimodal distribution. This observation can be attributed to the reduction in the strength of the particles, resulting in more breakage. Dhenge et al. (2012) similarly observed a reduction in consolidation and breakage with an increase in binder viscosity.

The sensitivity of the CQAs to these material properties suggests that additional experimental work should focus on characterizing powders, with particular emphasis on their strength, surface properties, and ability to absorb liquid. Further, the effects of these properties on the key inputs to DEM, such as the coefficients of restitution and friction, Poisson's ratio, and Young's modulus, should be investigated.

4. Summary and future work

A multi-scale model was developed and applied to a twin screw wet granulation process with mechanistic representations of aggregation, breakage, and consolidation. The model combines PBM and DEM techniques to predict the effects of equipment geometry, material properties, and process parameters on the CQAs of the product, building a knowledge space for QbD.

Results were reproducible and consistent with experimental trends. The screw element configuration determined the dominant

rate processes and strongly influenced the product attributes, with mixing elements resulting in more aggregation, breakage, and consolidation than the feed screw, forming larger, denser particles. The model also demonstrated sensitivities to screw speed, liquid-to-solid ratio, and material properties.

During design and scale-up, process engineers typically struggle to characterize the effects of process and design parameters on quality attributes, often relying on rules of thumb or simplistic scale-up methods. By establishing the sensitivities of the product quality to the process design, this work addresses the problem from a fundamental perspective, laying out a path for QbD and scale-up.

Future work will involve enhancing the model to account for the presence of fine powder particles and the mechanisms of nucleation and layering. Additionally, spatial compartments and particle flow can be included to simulate a more realistic process. Qualitative and quantitative validation with experimental results can then be performed, along with a thorough characterization of the relevant material properties.

Acknowledgments

This work is supported by the National Science Foundation Engineering Research Center on Structured Organic Particulate Systems Grant NSF-ECC 0540855 and Process Systems Enterprise. The authors also thank Jianfeng Li (Process Systems Enterprise), Jim Litster (Purdue University), and David Slade (Process Systems Enterprise) for contributing to discussions on this work.

References

- Ai, J., Chen, J.-F., Rotter, J.M., Ooi, J.Y., 2011. Assessment of rolling resistance models in discrete element simulations. *Powder Technol.* 206 (3), 269–282.
- Barrasso, D., ElHagrasly, A., Litster, J.D., Ramachandran, R. Multi-dimensional population balance model development and validation for a twin screw granulation process. *Powder Technol.*, <http://dx.doi.org/10.1016/j.powtec.2014.06.035>, in press.
- Barrasso, D., Ramachandran, R., 2012. A comparison of model order reduction techniques for a four-dimensional population balance model describing multi-component wet granulation processes. *Chem. Eng. Sci.* 80, 380–392.
- Barrasso, D., Ramachandran, R. Multi-scale modeling of granulation processes: Bi-directional coupling of PBM with DEM via collision frequencies. *Chem. Eng. Res. Des.* <http://dx.doi.org/10.1016/j.cherd.2014.04.016>, in press.
- Barrasso, D., Tamrakar, A., Ramachandran, R., 2014. A reduced order PBM-ANN model of a multi-scale PBM-DEM description of a wet granulation process. *Chem. Eng. Sci.* 119, 319–329.
- Barrasso, D., Walia, S., Ramachandran, R., 2013. Multi-component population balance modeling of continuous granulation processes: a parametric study and comparison with experimental trends. *Powder Technol.* 241, 85–97.
- Bouffard, J., Bertrand, F., Chaouki, J., 2012. A multiscale model for the simulation of granulation in rotor-based equipment. *Chem. Eng. Sci.* 81, 106–117.
- Braumann, A., Kraft, M., Mort, P.R., 2010. Parameter estimation in a multidimensional granulation model. *Powder Technol.* 197 (3), 196–210.
- Cameron, I., Wang, F., Immanuel, C., Stepanek, F., 2005. Process systems modelling and applications in granulation: A review. *Chem. Eng. Sci.* 60 (14), 3723–3750.
- CD-adapco, 2014. STAR-CCM+ v9.02 User Guide.
- Chaudhury, A., Barrasso, D., Pandey, P., Wu, H., Ramachandran, R., 2014a. Population balance model development, validation, and prediction of cQAs of a high-shear wet granulation process: Towards QbD in drug product pharmaceutical manufacturing. *J. Pharm. Innov.* 9 (1), 53–64.
- Chaudhury, A., Kapadia, A., Prakash, A.V., Barraso, D., Ramachandran, R., 2013. An extended cell-average technique for a multi-dimensional population balance of granulation describing aggregation and breakage. *Adv. Powder Technol.* 24 (6), 962–971.
- Chaudhury, A., Wu, H., Khan, M., Ramachandran, R., 2014b. A mechanistic population balance model for granulation processes: effect of process and formulation parameters. *Chem. Eng. Sci.* 107, 76–92.
- Cundall, P., Strack, O., 1979. Discrete numerical model for granular assemblies. *Geotechnique* 29 (1), 47–65.
- Darelius, A., Rasmuson, A., Björn, I.N., Folestad, S., 2005. High shear wet granulation modelling—a mechanistic approach using population balances. *Powder Technol.* 160 (3), 209–218.
- Dhenge, R.M., Cartwright, J.J., Hounslow, M.J., Salman, A.D., 2012. Twin screw granulation: steps in granule growth. *Int. J. Pharm.* 438 (12), 20–32.
- El Hagrasly, A., Hennenkamp, J., Burke, M., Cartwright, J., Litster, J., 2013. Twin screw wet granulation: influence of formulation parameters on granule properties and growth behavior. *Powder Technol.* 238, 108–115.
- Ennis, B.J., Tardos, G., Pfeffer, R., 1991. A microlevel-based characterization of granulation phenomena. *Powder Technol.* 65 (13), 257–272.
- Freireich, B., Litster, J., Wassgren, C., 2009. Using the discrete element method to predict collision-scale behavior: a sensitivity analysis. *Chem. Eng. Sci.* 64 (15), 3407–3416.
- Gantt, J.A., Cameron, I.T., Litster, J.D., Gatzke, E.P., 2006. Determination of coalescence kernels for high-shear granulation using DEM simulations. *Powder Technol.* 170 (2), 53–63.
- Goldschmidt, M., Weijers, G., Boerefijn, R., Kuipers, J., 2003. Discrete element modelling of fluidised bed spray granulation. *Powder Technol.* 138 (1), 39–45.
- Hassanpour, A., Ghadiri, M., 2004. Distinct element analysis and experimental evaluation of the heckel analysis of bulk powder compression. *Powder Technol.* 141 (3), 251–261.
- Immanuel, C.D., Doyle III, F.J., 2005. Solution technique for a multi-dimensional population balance model describing granulation processes. *Powder Technol.* 156 (23), 213–225.
- Ingram, G.D., Cameron, I.T., 2005. Formulation and comparison of alternative multiscale models for drum granulation. *Comput. Aided Chem. Eng.* 20, 481–486.
- Iveson, S., Litster, J., 1998. Liquid-bound granule impact deformation and coefficient of restitution. *Powder Technol.* 99 (3), 234–242.
- Iveson, S.M., Litster, J.D., Hapgood, K., Ennis, B.J., 2001. Nucleation, growth and breakage phenomena in agitated wet granulation processes: a review. *Powder Technol.* 117 (12), 3–39.
- Kayrak-Talay, D., Dale, S., Wassgren, C., Litster, J., 2013. Quality by design for wet granulation in pharmaceutical processing: assessing models for a priori design and scaling. *Powder Technol.* 240, 7–18.
- Liu, L., Smith, R., Litster, J., 2009. Wet granule breakage in a breakage only high-shear mixer: effect of formulation properties on breakage behaviour. *Powder Technol.* 189 (2), 158–164.
- Liu, L.X., Litster, J.D., Iveson, S.M., Ennis, B.J., 2000. Coalescence of deformable granules in wet granulation processes. *AIChE J.* 46 (3), 529–539.
- Man, P.L., Braumann, A., Kraft, M., 2010. Resolving conflicting parameter estimates in multivariate population balance models. *Chem. Eng. Sci.* 65 (13), 4038–4045.
- Mangwandi, C., Cheong, Y., Adams, M., Hounslow, M., Salman, A., 2007. The coefficient of restitution of different representative types of granules. *Chem. Eng. Sci.* 62 (12), 437–450.
- Poon, J.M.-H., Immanuel, C.D., Doyle III, F.J., Litster, J.D., 2008. A three-dimensional population balance model of granulation with a mechanistic representation of the nucleation and aggregation phenomena. *Chem. Eng. Sci.* 63 (5), 1315–1329.
- Ramachandran, R., Barton, P.I., 2010. Effective parameter estimation within a multi-dimensional population balance model framework. *Chem. Eng. Sci.* 65 (16), 4884–4893.
- Ramachandran, R., Immanuel, C.D., Stepanek, F., Litster III, F.J.D., 2009. A mechanistic model for breakage in population balances of granulation: theoretical kernel development and experimental validation. *Chem. Eng. Res. Des.* 87 (4), 598–611.
- Reinhold, A., Briesen, H., 2012. Numerical behavior of a multiscale aggregation model—coupling population balances and discrete element models. *Chem. Eng. Sci.* 70, 165–175.
- Sen, M., Barraso, D., Singh, R., Ramachandran, R., 2014. A multi-scale hybrid CFD-DEM-PBM description of a fluid-bed granulation process. *Processes* 2 (1), 89–111.
- Smith, R.M., Liu, L.X., Litster, J.D., 2010. Breakage of drop nucleated granules in a breakage only high shear mixer. *Chem. Eng. Sci.* 65 (21), 5651–5657.
- Tardos, G.I., Khan, M.I., Mort, P.R., 1997. Critical parameters and limiting conditions in binder granulation of fine powders. *Powder Technol.* 94 (3), 245–258.
- U.S. Food and Drug Administration, May 2006. Guidance for Industry: Q8 Pharmaceutical Development.
- U.S. Food and Drug Administration, November 2009. Guidance for Industry: Q8(R2) Pharmaceutical Development.
- van den Dries, K., Vromans, H., 2002. Relationship between inhomogeneity phenomena and granule growth mechanisms in a high-shear mixer. *Int. J. Pharm.* 247 (12), 167–177.
- Verkoeijen, D., Pouw, G.A., Meesters, G.M.H., Scarlett, B., 2002. Population balances for particulate processes a volume approach. *Chem. Eng. Sci.* 57 (12), 2287–2303.